Review of Scientific Instruments

A novel device for *in situ* study of gas adsorption under rotation

Cite as: Rev. Sci. Instrum. **92**, 045106 (2021); https://doi.org/10.1063/5.0039956
Submitted: 08 December 2020 • Accepted: 26 March 2021 • Published Online: 12 April 2021

R. I. Kosheleva, T. D. Karapantsios, M. Kostoglou, et al.

Review of Scientific Instruments ARTICLE scitation.org/journal/rsi

A novel device for *in situ* study of gas adsorption under rotation

Cite as: Rev. Sci. Instrum. 92, 045106 (2021); doi: 10.1063/5.0039956
Submitted: 8 December 2020 • Accepted: 26 March 2021 •
Published Online: 12 April 2021

R. I. Kosheleva,[1,2,a)] T. D. Karapantsios,[1] M. Kostoglou,[1] and A. Ch. Mitropoulos[2]

AFFILIATIONS

[1] Department of Chemical Technology and Industrial Chemistry, Faculty of Chemistry, Aristotle University, University Box 116, 541 24 Thessaloniki, Greece

[2] Hephaestus Advanced Laboratory, International Hellenic University, GR-654 04 Kavala, Greece

[a)] **Author to whom correspondence should be addressed:** kosheleva.ramonna@gmail.com

ABSTRACT

The effect of rotation on adsorption kinetics of CO_2 on activated carbon (AC) is studied using a novel rotation device. The device consists of a rotating cylindrical cell with inner dimensions of 4.5 cm radius and 1 mm height, while it operates at 5000 and 8000 rpm. Various cases of the CO_2/AC system are examined under a rotation field: in particular, (a) solid at vacuum, (b) gas without solid, (c) gas/solid at a non-equilibrium state of the adsorption process, and (d) gas/solid near an equilibrium state of the adsorption process. Micro-fragmentation of solid particles is observed at 8000 rpm but not at 5000 rpm; the latter is then chosen as the preferable speed for the rest of the experiments. During rotation of the gas, a well is noticed at the pressure curve, the size of which is in accordance with theoretical predictions of the behavior of a spinning gas. Rotation at an early stage of the adsorption process can suppress the filling time of a rotating storage reservoir to half of its value. Rotation near the equilibrium point reveals an enhanced adsorption capacity of the solid. The physics behind these phenomena are discussed with the aid of N_2-adsorption porosimetry and scanning electron microscopy measurements.

I. INTRODUCTION

Rotation plays an important role in the intensification of many industrial processes. On this account, a rotating packed bed (RPB) is often employed to accelerate the process.[1–3] This method has shown to increase the production efficiency, while an overall reduction in industrial size equipment is achieved. Distillation,[4] polymerization,[5] mixing,[6] multiphase mass transfer,[7] absorption for removal of gas pollutants,[8] and desorption[9] are only a few examples of such processes.

Although RPB has been thoroughly examined in gas–liquid,[10,11] liquid–liquid,[12,13] and liquid–solid[14,15] systems, there are only a few studies on gas–solid[16] systems and so far there are no studies at all on the fundamentals of the gas adsorption process under rotation at a constant volume. In a previous study,[17] we have examined the effect of rotation on vapor adsorption on Vycor glass by small-angle x-ray scattering coupled with the contrast matching technique. It was found that rotation results in a more stable thermodynamic configuration of the adsorbed film. Gao *et al.*[18] have investigated gas flow characteristics in RPB by particle image velocimetry. They concluded that the gas velocity and turbulent kinetic energy increased at outer and inner packing zones, respectively. Geyko and Fisch[19] have theoretically studied the spinning of an ideal gas in a cylinder with smooth surfaces under longitudinal and perpendicular compression to the rotating axis. They concluded that the spinning gas exhibits reduced compressibility because energy can be stored in the rotation.

Li *et al.*[20] performed experiments of phenol adsorption on activated carbon. Experimental results were modeled, and important parameters were highlighted. The study concluded that rotation enhances intra-particle diffusion by 1.48 times compared to conventional packed beds, while phenol molecules' interaction was increased due to rotation. However, Lukin *et al.*[21] have pointed out that although RPB is technically a promising alternative for product recovery, its economic benefits are questionable and further research on RPB technology is suggested.

In this work, a new device for the study of gas-to-solid adsorption kinetics under a rotational field is showcased. In contrast to RPB, the present device is designed to study the effect of rotation under constant volume, i.e., without the presence of a gas flow. Activated carbon (AC) is used as the adsorbent and CO_2 as the adsorbate. Measurements are organized in the following sections. First,

the effect of rotation on the adsorbent in vacuum is investigated. Then, the effect of rotation on the spinning gas is examined. Next, the effect of rotation on the adsorption process at a non-equilibrium stage is considered. Finally, the effect of rotation on the adsorption process near equilibrium is studied. Scanning electron microscope (SEM) micrographs before and after rotations are collected, and N_2-adsorption isotherms are recorded to supplement the analysis of the data.

II. DESIGN

Figure 1 shows the device, which consists of a sample cell, a vertical rotary motor, a pressure transducer, two valves, and a slip ring. The device is supported on a three-leg fixed table, while the slip ring is fixed on a hollow cylinder where a pressure transducer is housed in. The bottom part of the sample cell is mounted on the vertical rotary motor, while the top part can be moved upwards and downwards in order to place the adsorbent inside the cell [Fig. 1(a)]. The sample cell is closed by six screws in the periphery of the top part, while sealing is achieved by two O-rings inside the cell.

When the cell is tightly closed, a space of 1 mm height and 90 mm diameter is available for the sample material. On the top part of the cell, there are two valves placed symmetrically that serve as gas inlet–outlet ports. In the center of the top part, the pressure transducer (PV7004, ifm electronics) is connected, which is capable of recording absolute pressure at prescribed time intervals (down to ms^{-1}) with accuracy ±0.5% and repeatability ±0.05% of the span [Fig. 1(b)]. The slip ring on top of the main assembly allows the transducer to be wired and connected to a PC for on-line pressure monitoring and recording. Complimentary parts of the set up are a reservoir vessel and an oil-free vacuum pump; all are connected to the main device by tubes [Fig. 1(c)].

The system is designed to operate in a range of conditions regarding temperature and pressure. Specifically, measurements can be conducted at temperatures from −20 to 30 °C inside an insulated container. Temperature below 15 °C is regulated with coolant circulation, while above that value, a fan heater is used. Pressure can range from vacuum conditions (10^{-2} bar) up to 10 bars, and gas dosage is regulated by a connected vessel of known volume, which serves as a reservoir tank. The rotary motor operates at two rotational speeds, 5000 and 8000 rpm, when the sample cell is loaded.

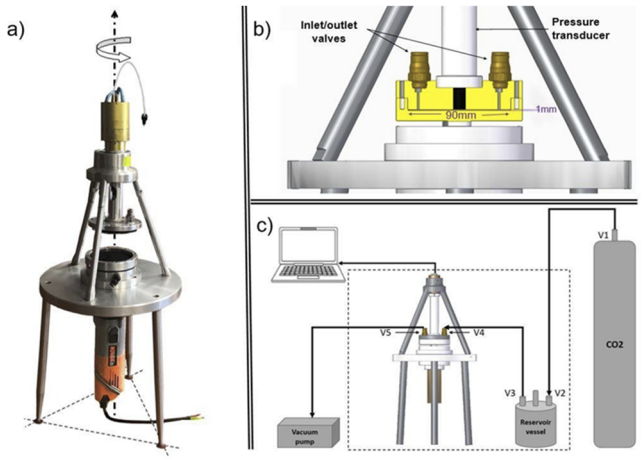

FIG. 1. (a) Image of the device, (b) schematic cross section of the sample cell, and (c) schematic representation of the experimental setup; the dashed line frame represents the insulated container, while V (1–5) stands for existing valves. A vacuum pump can be connected interchangeably to any part of the system.

III. EXPERIMENTAL DETAILS

Commercially available activated carbon (AC), in grains with size of about 100 μm, and CO_2 of high purity (99%) are used in this study. Figure 2 shows the N_2-adsorption isotherms at 77 K (−196 °C) on a fresh AC sample and on an AC sample after rotation measured with a Nova Quantochrome porosimeter. The result is an adsorption isotherm of the amount adsorbed per mass unit of the material (cm^3/g) at standard temperature and pressure (STP) vs relative pressure p/p_0, where p_0 is the saturation vapor pressure of N_2. For the fresh AC, the BET (Brunauer, Emmett, and Teller) surface area is estimated to be equal to 1110 m^2/g and the average pore size, based on the BJH (Barrett, Joyner, and Halenda) method,[22] is ~16.3 Å.

The volume of liquid N_2, near to the saturation point (~p/p_0 = 1) of the isotherm, is taken to be equal to the volume of the AC particle porosity (intra-porosity) V_{intra} = 0.632 cm^3/g. Since the geometrical volume, calculated as the volume of a cylinder of r = 4.5 cm and h = 0.1 cm, of the rotating cell is V_{cell} = 6.36 cm^3 and the mass of AC grains filling it is m_{gr} = 3.6 g, the volume occupied

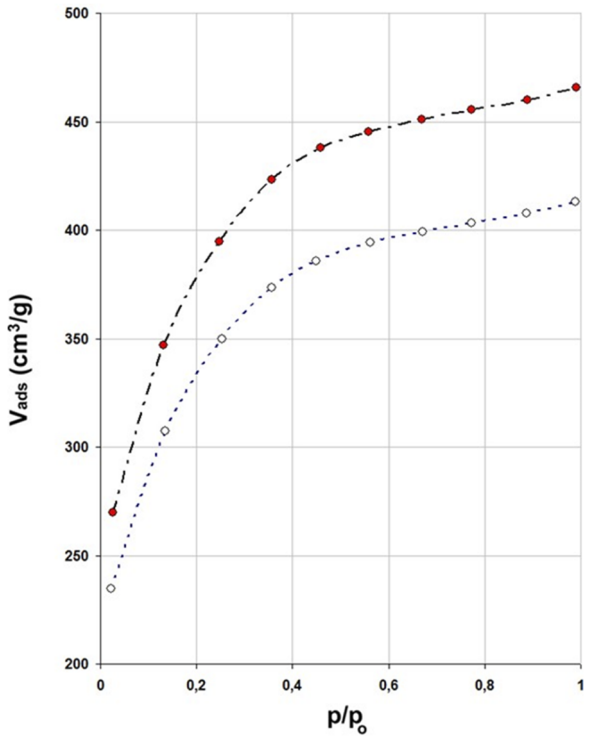

FIG. 2. N_2-adsorption isotherm on AC at 77 K. Open circles are for the fresh sample. Solid circles are values of the rotated sample at 5000 rpm.

by grains is V_{gr} = 4.08 cm^3. By assuming the skeletal density of AC ρ_s = 2 g/cm^3,[23] the space between AC particles (inter-porosity) of the rotating bed is calculated from

$$\varepsilon_{inter} = \left[1 - \frac{V_{gr}}{V_{cell}}\right] \times 100 = 36\%. \quad (1)$$

Finally, intra-porosity is found from

$$\varepsilon_{intra} = \frac{\rho_s - \rho_{gr}}{\rho_s - \rho_g} \times 100 = 56\%, \quad (2)$$

where ρ_g is the gas density within pores; for empty pores, ρ_g = 0 g/cm^3. The density of grains including pores is ρ_{gr} = 0.882 g/cm^3. The result indicates a random close packing inside the cell.

IV. EXPERIMENTAL PROCEDURE

Prior to any measurement, the system is evacuated by opening all involved valves [V#, see Fig. 1(b)] for a sufficient period of time (overnight) to ensure the removal of any volatile impurities. After vacuum is achieved, V4 is closed and CO_2 is introduced to the reservoir vessel. Next, V5 is closed and the vacuum pump is turned off. The pressure and temperature inside the reservoir tank are monitored by a transducer; gas is fed into the sample cell by regulating V4. Finally, tubing is disconnected from the main device so that the sample cell rotates freely. For all cases, experiments are conducted at 20 °C.

First, the effect of rotational speeds on AC under vacuum was examined in order to determine if there are any structural alterations (i.e., fragmentation) as well as to designate the optimal rotational conditions. After the vacuum was achieved, rotation took place for 60 s both for 5000 and 8000 rpm. The total duration of each run was 10 min, and the pressure was recorded with an interval of 1 s. Supplementary SEM measurements for AC before (fresh sample) and after rotation were performed.

In order to understand how the gas behaves under rotation and what the interplay with the AC is, two runs were conducted: one with the sample cell free of AC and one loaded with the material. The steps before the run itself are the same with the above case and at the same temperature condition. Carbon dioxide was introduced in both cases at an initial pressure of 5500 mbar. Rotation of 5000 rpm was initiated after 5 min of CO_2 introduction with a duration of 60 s. The pressure was recorded for 11 min in total: 5 min before rotation, 1 min during rotation, and 5 more minutes after rotation stopped.

Finally, the experiment was set up to study the effect of rotation on CO_2 adsorption at near equilibrium, where ΔP was not observed anymore. The initial pressure of CO_2 was 5150 mbar and equilibrium was reached after 20 h of adsorption. At this point, rotation for 60 s at 5000 rpm took place. The system was left to rest, to more than 20 h after rotation ceased, until a subsequent equilibrium was achieved. Once again, the pressure was recorded through the experiment at an interval of 1 s.

V. MEASUREMENTS

A. Effect of rotation on solid

Figure 3 shows Scanning Electron Microscopy (SEM) micrographs depicting the effect of a 60 s rotation on the adsorbent under vacuum at the given two different rotational speeds, compared to the surface of fresh AC. The graph at the bottom left part shows the pressure profile during rotation at 5000 and 8000 rpm. The pressure was recorded for 11 min in total; however, the presented graph shows pressure records only for 3 min including the rotation of 60 s that took place at the fifth minute of the recording. In the case of 5000 rpm, there is a starting kick that lasts for ~20 s and after that the rotation pattern comes back to its original one. At 8000 rpm, the pattern is different; the system does not come back to its initial pressure, but continues into a higher path for reasons that are suggested next.

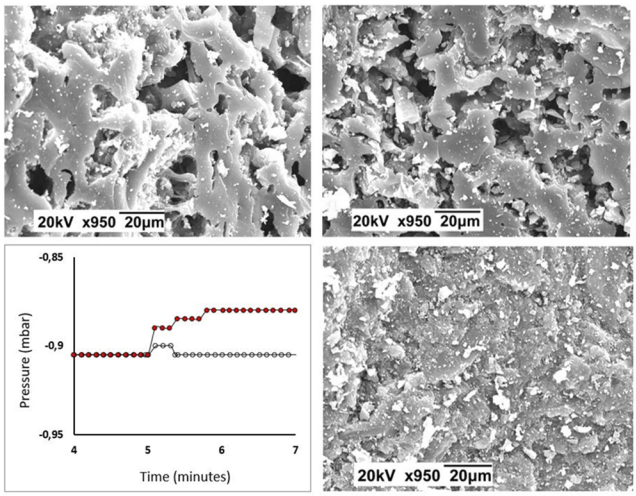

FIG. 3. SEM micrographs (20 kV; x950; 20 μm) and rotation curves of AC. Left: top, fresh AC; bottom, rotation curves: red circles at 8000 rpm, empty circles 5000 rpm (under vacuum). Right: top, AC after rotation at 5000 rpm; bottom, AC after rotation at 8000 rpm.

The rotated samples are examined by SEM and compared to a fresh AC sample. The result indicates that at 5000 rpm, the surface of the AC undergoes only a minor differentiation whereas at 8000 rpm a larger one. During rotation, the solid particle attains different Froude numbers (F_ω) for different angular velocities ω, that is,

$$F_\omega = \omega\sqrt{\frac{r}{g}}x\sqrt{\sin\beta_s\sqrt{\varepsilon_{intra}}}, \quad (3)$$

where g is the acceleration of gravity and $\sin\beta_s$ is the repose angle.[24]

In the case of 5000 rpm, the low friction indicates that β_s is small, i.e., the particles remain at their initial position; in other words, the bulk material does not undergo centrifugation (i.e., there is no friction). In the case of 8000 rpm, the SEM images suggest that there is some friction between the particles. As a result, a temporal increase in the pressure is observed before the system resumes its original state (Fig. 3, bottom left).

For situations where there is no centrifugation, $F_\omega < 1$. Therefore, from Eq. (3), and since at 5000 rpm no centrifugation is present, the relative Froude numbers between 8000 and 5000 rpm are equal to 1.6. These values are reasonable for a randomly close packed bed suggesting only slight movements (of the order of micrometers) of solid particles at 8000 rpm, and thus, a micro-fragmentation of

the rotating sample is possible. In order to avoid this complication, measurements at 5000 rpm are collected for the next parts of this study.

B. Effect of rotation on gas

Figure 4(a) shows the behavior of the spinning gas without adsorbent. Carbon dioxide is introduced to the cell at an initial pressure of 5500 mbar and rotation at 5000 rpm is conducted for 60 s after about 5 min from gas introduction. The temperature is kept constant at 20 °C. The rotation affects the gas pressure leading to a sudden pressure drop (rotating well), which soon comes to a rotation-induced steady state condition at a depth of about 25 mbar.

The rotation causes pressure redistribution between the center and the edge of the rotating cell in a way that

$$P(0) = P_{in}\frac{\phi}{e^{\phi}-1} \text{ and } P(r) = P(0)e^{\phi} \text{ with } \phi = \frac{M\omega^2 r^2}{2RT}, \quad (4)$$

where P_{in} is the initial pressure, P(0) and P(r) are the pressures at the center of the rotation axis and at distance r from it, respectively, and ϕ is the rotational exponent with M being the molecular weight of the rotating gas, ω being the angular velocity, R being the gas constant, and T being the absolute temperature.

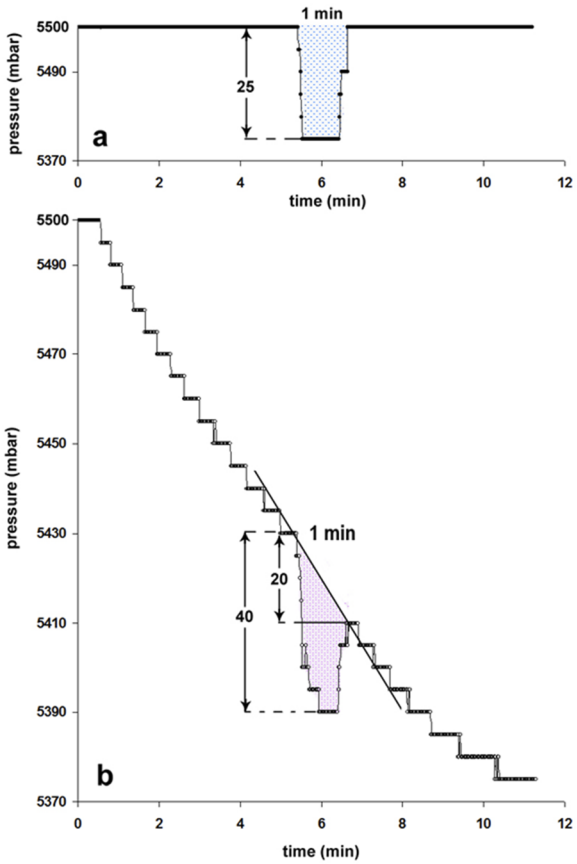

FIG. 4. (a) Gas spinning without adsorbent. (b) Gas/solid rotation at a non-equilibrium stage. In both cases, the rotation speed is 5000 rpm.

In this particular experiment, P_{in} = 5500 mbar, and for r = 4.5 cm, the rotational exponent is ϕ = 0.005, P(0) = 5486 mbar, and P(r) = 5514 mbar. Although differences are very subtle, the max–min pressure difference is in accordance to the theoretical rotating well depth, indicating the sensitivity of the device to register pressure variation.

Apparently, the magnitude of the pressure well depends mainly on the geometry of the rotating cell. The rotation exponent increases faster with increasing r than ω. Therefore, a different geometrical design can provide a greater depth for the well. For instance, if the radius of the rotating cell increases by one order of magnitude (i.e., from 5 to 50 cm), the spinning gas well will be more than 3000 mbar in depth.

C. Effect of rotation at a non-equilibrium adsorption stage of a gas/solid system

Figure 4(b) shows the behavior of the spinning gas in the presence of AC at a very early stage of the adsorption process, i.e., when the pores are almost empty. The pressure curve in this case is the outcome of the combination of the adsorption process and the spinning gas effect, resulting in a non-uniform well depth ranging from 40 to 20 mbar. During rotation in a non-equilibrium state, the surface coverage in time is given as

$$\frac{d\theta}{dt} = k_{ads}P(1-\theta) - k_{des}\theta, \quad (5)$$

where θ is the fractional surface coverage and k_{ads} and k_{des} are the adsorption and desorption constants, respectively.

At an early adsorption stage, θ is very small and the first part of the right-hand side in Eq. (5) dominates, i.e., the gas molecules are adsorbed very quickly in the empty pores. A simple estimation of the pressure drop rate for 1 min period before and after rotation shows a 10 mbar pressure drop, while during rotation, the pressure is decreased by 20 mbar for the same period of time [see ΔP of the pink shaded area in Fig. 4(b)]. Therefore, it is suggested that rotation can provide a solution for faster gas storage at a given pressure.

However, at a given pressure (i.e., in a batch process), as pores fill with adsorbed molecules, the adsorption rate will decrease and near to equilibrium, it will become slow. By increasing the pressure, the adsorption rate within the partially filled pores will increase again and this continues. That is, in a continue process, fast gas storage of a rotating reservoir can be attained.

The filling time of a reservoir on board is currently an important issue for hydrogen storage tank technology; the requirement is for 3 min. To meet this requirement, Zhou *et al.*[25] have suggested that the refueling parameters need to be investigated urgently. Reddi *et al.*[26] have also arrived at the same conclusion by reviewing the SAE J2601 re-fueling protocols.

D. Effect of rotation near adsorption equilibrium state of a gas solid system

Figure 5 shows the effect of rotation on the adsorption kinetics of CO_2 on AC. In the region from A to B, adsorption takes place and at point B, the system comes near to equilibrium where ΔP is no longer detected. The data of this region are fitted with a non-linear

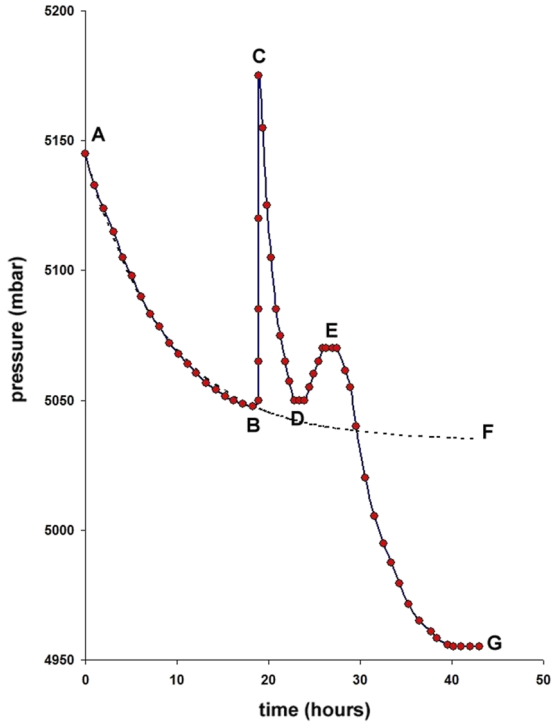

FIG. 5. Gas/solid rotation at 5000 rpm near equilibrium (for details, see the text).

pseudo-first-order (PFO) kinetic curve by least squares,

$$P_{th} = P_{eq} + (P_{in} - P_{eq})e^{-k_1 t}, \quad (6)$$

where P_{th} is the theoretical pressure to be compared with the experimental one, P_{eq} = 5035 mbar is the equilibrium pressure, P_{in} = PA = 5145 mbar, $k_1 = 0.115\ min^{-1}$ is the PFO rate constant, and t is the time. Since the saturation pressure of CO_2 at 20 °C is 57.29 bars, the system is initially at a relative pressure $p/p_0 = 0.09$.

There are differences in pressure behavior during rotation between non-equilibrium and near equilibrium cases. In the latter case, an abrupt pressure peak is formed (point C). Such a pressure increase is highly repeatable in all experiments conducted at room temperature and it is attributed to temporary gas desorption. This specific phenomenon is not observed in near equilibrium experiments at lower temperatures and further research is needed before conclusive statements can be made.

After rotation, the system tries to recover its initial equilibrium, but the previously desorbed gas, alongside with the initial bulk gas, is forced by backflow to make a long journey toward the center and back to the pores, resulting in slow kinetics. Region CDE is a resemblance of recalescence,[27,28] which is observed when an increase in entropy of the system takes place.

Although at point F the adsorption process theoretically should have reached equilibrium, it continues up to point G. The pressure difference between F and G indicates enhanced adsorption. The prime mechanism of this enhancement is that the rotation pushes CO_2 molecules to some inaccessible adsorptive sites that become now accessible. The suggested mechanism is supported by N_2 adsorption measurements of the material before and after rotation shown in Sec. III. Figure 2 compares the N_2-adsorption isotherm at 77 K of the fresh AC sample with that after rotation. The BET area is now 1173 m^2/g and the Gurvitsh volume is 0.726 cm^3/g in liquid N_2 corresponding to an increase of about 6% and 14% respectively from the initial values given in the experimental details section. However, the BJH pore size distribution from desorption brunch seems to be unchanged at 16.3 Å in accordance with the SEM result.

VI. CONCLUSIONS

In this work, a novel rotating device that allows studying the effect of rotation on gas adsorption kinetics is presented. Carbon dioxide and AC are used as the gas/solid system in order to exemplify the capabilities of the design. Rotation is conducted at two different speeds of 5000 and 8000 rpm at 20 °C. However, the second angular velocity of 8000 rpm was soon abandoned after it was noticed that it causes micro-fragmentation to the sample.

Gas rotation without the presence of a particles' packed bed is mainly governed by the geometry of the rotating cell. Gas/solid rotation at a non-equilibrium state of the adsorption process can accelerate the filling of a rotating storage reservoir to about half of the required time without rotation. Gas/solid rotation near equilibrium enhances the adsorptive capacity of the adsorbent.

Nitrogen porosimetry of fresh and rotating treated AC samples indicates an increase in both the internal surface area and pore volume. Since fragmentation does not contribute to the internal surface area and pore volume, the increments of about 60 m^2/g and 90 cm^3/g compared to the fresh sample is mainly attributed to the rotation. It is suggested that rotation may render accessible to a number of adsorptive sites, which were inaccessible prior to rotation.

The present device makes possible the investigation of the effect of rotation on the adsorption process under constant volume measurements, opening new paths toward gas storage technologies, while the proposed methodology offers a novel technique for characterizing materials and studying fundamentals of RPB and relevant technologies.

ACKNOWLEDGMENTS

Authors R.I.K. and A.C.M. would like to thank the project entitled "Development of NAnotechnology-enabled 'next-generation' MEmbranes and their applications in Low-Energy, zero liquid discharge Desalination membrane systems"/NAMED, Grant No. T2ΔΓΕ-0597 for funding. In addition, they would like to thank Mr. G. Bomis for the construction of the device.

NOMENCLATURE

F_ω	=	Froude number
h	=	inner height of the sample cell (cm)
k_{ads}	=	adsorption rate constant
k_{des}	=	desorption rate constant
k_1	=	adsorption kinetic rate (min^{-1})
m_{gr}	=	mass of the AC in the sample cell (g)
M	=	molar mass of the gas (g/mol)

P_{eq} = pressure at equilibrium (mbar)
P_{in} = initial pressure of the gas (mbar)
P_{th} = theoretical pressure withdrawn from the pseudo-first-order kinetic model (mbar)
P(r) = pressure of the gas at a radius from the center of the sample cell (mbar)
P(0) = pressure of the gas at the center of the sample cell (mbar)
r = inner radius of the sample cell (cm)
V_{cell} = volume of the sample cell (cm^3)
V_{gr} = volume occupied by AC grains (cm^3)
V_{intra} = volume of the intra-particle space (cm^3)

Greek letters

ΔP = pressure difference (mbar)
β_s = repose angle (rad)
ε_{inter} = inter-particle porosity (%)
ε_{intra} = intra-particle porosity (%)
θ = fractional surface coverage
ρ_g = the density of the gas (g/cm^3)
ρ_{gr} = the density of the AC grains (g/cm^3)
ρ_s = the density of the skeletal solid (g/cm^3)
ω = angular velocity (rad/s)

Abbreviations

AC = activated carbon
BET = Brunner, Emmet, and Teller
BJH = Barrett, Joyner, and Halenda
PFO = pseudo-first-order kinetic model
rpm = revolution per minute
SEM = scanning electron microscopy

DATA AVAILABILITY

The data that support the findings of this study are available within the article.

REFERENCES

[1]T.-L. Chen, Y.-H. Chen, and P.-C. Chiang, "Enhanced performance on simultaneous removal of NO_x-SO_2-CO_2 using a high-gravity rotating packed bed and alkaline wastes towards green process intensification," Chem. Eng. J. **393**, 124678 (2020).
[2]F. Zarei *et al.*, "Insight into the experimental and modeling study of process intensification for post-combustion CO_2 capture by rotating packed bed," J. Cleaner Prod. **211**, 953–961 (2019).
[3]D. Wang *et al.*, "Process intensification of quasi-homogeneous catalytic hydrogenation in a rotating packed bed reactor," Ind. Eng. Chem. Res. **59**, 1383–1392 (2019).
[4]H. Qammar *et al.*, "Experimental investigation and design of rotating packed beds for distillation," Chem. Eng. Trans. **69**, 655–660 (2018).
[5]X. Liu *et al.*, "Controllable polymerization of *n*-butyl cyanoacrylate using a high-gravity rotating packed bed," Chem. Eng. J. **379**, 122400 (2020).
[6]Y. Ouyang *et al.*, "Micromixing efficiency in a rotating packed bed with non-Newtonian fluid," Chem. Eng. J. **354**, 162–171 (2018).
[7]C.-C. Lin and Y.-W. Kuo, "Mass transfer performance of rotating packed beds with blade packings in absorption of CO_2 into MEA solution," Int. J. Heat Mass Transfer **97**, 712–718 (2016).
[8]H. Zou *et al.*, "Removal of hydrogen sulfide from coke oven gas by catalytic oxidative absorption in a rotating packed bed," Fuel **204**, 47–53 (2017).
[9]Q. Guo *et al.*, "Adsorption and desorption behaviour of toluene on activated carbon in a high gravity rotating bed," Chem. Eng. Res. Des. **143**, 47–55 (2019).
[10]X. Lu *et al.*, "A porous media model for CFD simulations of gas-liquid two-phase flow in rotating packed beds," Chem. Eng. Sci. **189**, 123–134 (2018).
[11]Y. Yang *et al.*, "CFD modeling of gas–liquid mass transfer process in a rotating packed bed," Chem. Eng. J. **294**, 111–121 (2016).
[12]H. Huang *et al.*, "Effect of temperature on gas adsorption and separation in ZIF-8: A combined experimental and molecular simulation study," Chem. Eng. Sci. **66**, 6297–6305 (2011).
[13]L. Liang *et al.*, "Liquid nitrogen freezing method for exploring the mixing characteristics of liquid/liquid heterogeneous in outer packing cavity of impinging stream-rotating packed bed," Chem. Eng. Process.–Process Intensif. **150**, 107906 (2020).
[14]J. A. Hacking *et al.*, "Improving liquid distribution in a rotating packed bed," Chem. Eng. Process.–Process Intensif. **149**, 107861 (2020).
[15]Y. Liu *et al.*, "Liquid microflow inside the packing of a rotating packed bed reactor: Computational, observational and experimental studies," Chem. Eng. J. **386**, 121134 (2020).
[16]J.-Q. Wang *et al.*, "CFD analysis of gas flow characteristics in a rotating packed bed with randomly arranged spherical packing," Chem. Eng. J. **385**, 123812 (2020).
[17]R. I. Kosheleva *et al.*, "A rotating sample cell for *in situ* measurements of adsorption with x-rays," Rev. Sci. Instrum. **89**, 123113 (2018).
[18]X.-Y. Gao *et al.*, "Gas flow characteristics in a rotating packed bed by particle image velocimetry (PIV) measurement," Ind. Eng. Chem. Res. **56**, 14350–14361 (2017).
[19]V. I. Geyko and N. J. Fisch, "Reduced compressibility and an inverse problem for a spinning gas," Phys. Rev. Lett. **110**, 150604 (2013).
[20]W. Li *et al.*, "Adsorption of phenol by activated carbon in rotating packed bed: Experiment and modeling," Appl. Therm. Eng. **142**, 760–766 (2018).
[21]I. Lukin *et al.*, "Economic evaluation of rotating packed bed use for aroma absorption from bioreactor off-gas," Chem. Eng. Process.–Process Intensif. **154**, 108011 (2020).
[22]E. P. Barrett, L. G. Joyner, and P. P. Halenda, "The determination of pore volume and area distributions in porous substances. I. Computations from nitrogen isotherms," J. Am. Chem. Soc. **73**, 373–380 (1951).
[23]D. R. Lide, *CRC Handbook of Chemistry and Physics* (CRC Press, 2004), Vol. 85.
[24]G. Juarez, P. Chen, and R. M. Lueptow, "Transition to centrifuging granular flow in rotating tumblers: A modified Froude number," New J. Phys. **13**, 053055 (2011).
[25]L. Zhou, "Progress and problems in hydrogen storage methods," Renewable Sustainable Energy Rev. **9**, 395–408 (2005).
[26]K. Reddi *et al.*, "Impact of hydrogen SAE J2601 fueling methods on fueling time of light-duty fuel cell electric vehicles," Int. J. Hydrogen Energy **42**, 16675–16685 (2017).
[27]Y. Nakano and A. Hashimoto, "Bubbles to chondrites-I. Evaporation and condensation experiments, and formation of chondrules," Prog. Earth Planet. Sci. **7**, 47 (2020).
[28]L. Sang *et al.*, "The influence of cooling rate on the microstructure and phase fraction of gas atomized $NiAl_3$ alloy powders during rapid solidification," Vacuum **157**, 354–360 (2018).